Proceedings of the ASME 2014 Dynamic Systems and Control Conference
DSCC 2014
October 22-24, 2014, San Antonio, Texas, USA

DSCC2014-6027

A PASSIVE UPPER LIMB EXOSKELETON FOR MACAQUES IN A BMI STUDY – KINEMATIC DESIGN, ANALYSIS, AND CALIBRATION*

Junkai Lu, Wenjie Chen,† Kevin Haninger, and Masayoshi Tomizuka
Dept. of Mechanical Engineering
University of California
Berkeley, California 94720
Email: {junkai.lu, wjchen, khaninger, tomizuka}@berkeley.edu

ABSTRACT

Integrating an exoskeleton as an external apparatus for a brain-machine interface has the advantage of providing multiple contact points to determine body segment postures and allowing control to and feedback from each joint. When using macaques as subjects to study neural control of movement, a singularity-free upper limb exoskeleton is required to guarantee safe and accurate tracking of joint angles over all possible range of motion. In addition, the compactness of a design is of more importance considering macaques' significantly smaller body dimensions than humans'. Proposed in this paper is a 6-degree-of-freedom (DOF) passive upper limb exoskeleton with 4 DOFs at the shoulder complex. System kinematic analysis is investigated in terms of its singularity and manipulability. A real-time data acquisition system is set up, and system kinematic calibration is conducted.

INTRODUCTION

Brain-machine interfaces (BMIs) can provide means to enable communication between the brain and the outside world. They are often aimed at assisting, augmenting, or repairing human cognitive or sensory-motor functions, especially for paralyzed patients. Researchers have used BMIs to allow able-bodied monkeys [1] and humans suffering from brainstem stroke [2] to control robotic arms in 3D reach and grasp tasks, which have helped promote a new paradigm of human-robot interaction.

On the other hand, traditional human-robot interaction is well established in the rehabilitation field. Particularly for upper limb rehabilitation, most existing therapy robots are either end-effector-based or exoskeleton devices [3]. Since an end-effector-based robot generally interacts with patients through only one point, it fails to fully determine the arm postures and the interaction torques at each joint. A wearable exoskeleton, although having a more complicated mechanical structure and system dynamics, has multiple contact points with the subject's body, allowing control to and feedback from each joint individually. An exoskeleton may more effectively restore patient's mobility with control of the affected limbs shared between the exoskeleton controller and the patient's residual motor control abilities. Since the exoskeleton is capable of embedding itself into patient's body schema and providing somatosensory and proprioceptive feedbacks that are consistent with patient's limb movements, it allows more natural motion.

Per the above discussions, an exoskeleton as an apparatus controlled by the BMI may more closely match natural motion, which may allow better study of the neural control of movement. Studies have shown that more invasive animal experiments generally produce higher performance than human cases [4], and that currently microelectrode array is the only recording technique which allows decoding the subject's intended limb movements with high accuracy [5]. Thus we propose an invasive BMI system using microelectrode arrays with rhesus macaques (*Macaca mulatta*) as the study subjects, using the involved exoskeleton that operates in a 3D workspace to help establish a closed-loop BMI and to enable subjects' proprioceptive feedback. In the first

*THIS WORK WAS SUPPORTED BY NSF EFRI GRANT #1137267.
†Currently with FANUC Corporation.

stage, passive kinematic motion data acquisition is one of the major exoskeleton tasks. To achieve this, a compact exoskeleton design with a singularity-free shoulder joint is needed for guaranteeing both precise tracking and safety.

In this paper, a 6-DOF upper limb exoskeleton model with 4 DOFs at the shoulder complex is proposed to achieve better manipulability than conventional triad (3 DOFs) shoulder models, and a non-motorized prototype design is built working as a kinematic motion sensing device for offline neural decoding studies as well as for animal training purposes. This paper is organized as follows: preliminaries of primate upper limb modeling, kinematic design difficulties and state-of-the-art are first introduced; the exoskeleton system design is then presented including proposed modeling, mechanical design, and real-time data acquisition; kinematic analysis of the proposed shoulder joint model is discussed by investigating the model's manipulability, and system kinematic calibration is conducted with the help of an external motion capture system; finally, conclusions of this paper and some future work are discussed.

PRELIMINARIES

Currently, the KINARM introduced in [6] is the only upper limb exoskeleton designed for non-human primates. It is a 2-DOF actuated device allowing for movement in a 2D plane. Most of the existing upper limb exoskeletons for 3D workspaces are dedicated to human rehabilitation, and their target functions and design requirements are different from what we would like to achieve. However, they can still serve as pilot examples to investigate.

Kinematic Design Difficulties

Kinematic design is one of the key aspects for developing an upper limb exoskeleton, and to match a mechanical exoskeleton to a biological structure faces difficulties, especially in the shoulder complex. Specifically, two major problems are axis alignment between the anatomical and device joints and the kinematic singularity of mechanical models. The former problem arises with the fact that the shoulder center of rotation changes as a function of posture [7]. This can be explained by Fig. 1, which shows that the shoulder complex is a highly-coupled mechanism of great complexity. It consists of four joints, and each joint possesses multiple DOFs [8]. A large amount of research has been conducted to reduce joint axis misalignment to guarantee user's range of motion (ROM) and comfort [3, 9, 10].

The other kinematic design difficulty is how to avoid the mechanical model singularities of the shoulder complex. A *kinematic singularity* refers to a configuration in which there is a change in the number of instantaneous DOFs, and the mechanism cannot move arbitrarily. This is highly undesirable for a motion tracking system. In the vicinity of a singularity for a motorized

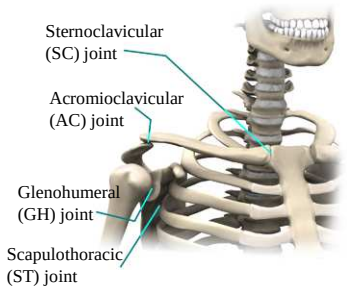

FIGURE 1: JOINTS LOCATED AT THE SHOULDER COMPLEX. [11]

design, small desired velocities in the task space will require very large joint motions if the task space velocities have components along the degenerated directions. These large joint motions may damage the motors or even result in severe injuries to the user. Apart from axis alignment DOFs, the shoulder complex can be basically modeled by a ball-and-socket joint consisting of three rotational DOFs, which can be mechanically implemented using three serial revolute joints. Two conventions shown in Fig. 2 are widely used to describe the rotation sequence [12]. However, since both conventions use a triad model, singularities cannot be avoided if their postures require an alignment of their first joint axis with the third.

Compared with the axis alignment problem, the singularity issue in the shoulder complex design has not drawn the same amount of attention since rehabilitation-oriented exoskeletons typically do not require large ROM, and the training motions for patients are expected to be within certain patterns. Thus mechanism singularities can be intentionally avoided. However, for an exoskeleton designed for a macaque, when operated in the passive tracking mode where the macaque's arm is free to do arbitrary motion, a singularity-free design of the shoulder complex is of significance for allowing precise tracking and addressing safety concerns, considering macaques are generally non-cooperative. To allow alignment between the exoskeleton and the macaque, more DOFs would need to be added to the shoulder complex, but this will increase the total complexity, especially for a totally passive mechanism design. In fact the compactness of a macaque exoskeleton is another kinematic design difficulty researchers have to solve due to macaques' small dimensions [13], which will also be detailed later. Since the requirement of a compact design limits the allowable complexity, only the kinematic singularity of the shoulder model is considered here.

State-of-the-Art

To reduce the occurrence of kinematic singularities, several research groups revised the aforementioned standard triad models based on different concerns and assumptions. Typical designs

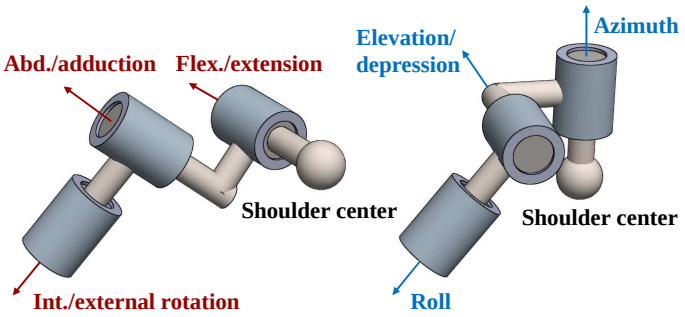

(a) flexion-abduction-rotation (b) azimuth-elevation-roll

FIGURE 2: TWO ROTATION CONVENTIONS FOR GH JOINT MODEL.

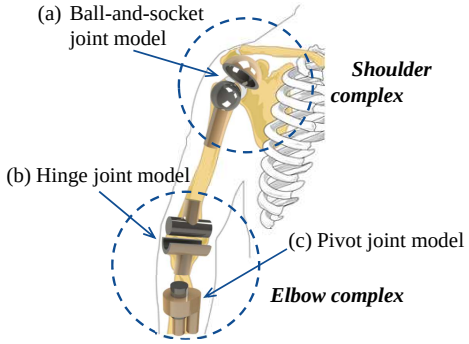

FIGURE 3: MECHANICAL MODELS OF THE UPPER LIMB JOINTS.

are (CADEN)-7 [14], MEDARM [9], and SAM [15]. (CADEN)-7 used a strategy of assigning the mechanism's singularity to a direction that is anthropometrically hard to reach in human's activities of daily living (ADL). In this way, it was claimed that the majority of the exoskeleton workspace is free of singularities. MEDARM utilized an optimization-based approach to define the relative angle between its first joint axis and the second. Using the proposed parameters, it was claimed there is no singularity in their prescribed workspace. SAM is an intermediate design between (CADEN)-7 and MEDARM considering its first joint axis configuration as well as using the condition number of the Jacobian matrix (isotropic index) to evaluate system manipulability. However, all these designs used a triad joint model to mimic the shoulder complex, making each task space posture correspond to a unique inverse solution for the joint space realization, therefore a singularity always exists.

Mechanical Models of Upper Limb Joints

The functionality of primate upper limbs is determined by the shoulder complex, elbow complex, wrist, and hand.

The shoulder complex is one of the most difficult structures to model for an upper limb. Although [16] points out that the morphology of the macaque shoulder joint is not exactly the same as a human's, human upper limb structure can still serve as a reference for developing the kinematic design of an exoskeleton since there are no macaque shoulder joint models in existing literature. [17] introduces a non-redundant 5-DOF mathematical model of the shoulder complex for humans including three rotational DOFs (abduction/adduction, flexion/extension, and internal/external rotation) and two translational DOFs (elevation/depression, and protraction/retraction) with thorax as the fixed base. However, in the engineering world, for simplicity, mostly only the glenohumeral joint (Fig. 1) is modeled for the shoulder complex using a ball-and-socket joint model, as shown in Fig. 3a. The elbow complex mainly consists of the elbow joint and the radioulnar joint. The former is commonly modeled using a hinge joint as shown in Fig. 3b, and the latter is generally regarded as a pivot joint corresponding to pronosupination of the forearm as shown in Fig. 3c. This DOF can be included either with the elbow or the wrist, and serves as a revolute joint connecting the elbow and the wrist.

In the current stage of this project, we assume that the macaque is allowed to freely use its hand to press/grasp targets without the exoskeleton components on the wrist or the hand, i.e., the distal DOFs of the upper limb are not included in the exoskeleton design. Thus the wrist and the hand motions and their modeling are not investigated in this paper.

EXOSKELETON SYSTEM DESIGN

The designed BMI task for macaques is shown in Fig. 4. A macaque is seated in a chair with its collar and torso constrained, and the proposed exoskeleton is attached to the macaque's right upper limb for passively following and recording the voluntary motion of the arm to reach/grasp targets in the 3D presentation system. In this section, the exoskeleton system design will be presented.

Design Requirements

Singularity-free Design As previously discussed, an exoskeleton with singularity-free design of shoulder complex is required for both large joint ROM and safety considerations. Although the safety issue is not as critical in a fully passive mechanism, it will be one of the major concerns in the control of a future motorized design.

Compact Design The compactness is also of importance to an upper-limb exoskeleton designed for macaques. Table 1 lists the key body dimensions of our BMI macaques in comparison to those of human, which suggests that the space around the macaque upper-limbs is quite limited. Thus mechanical com-

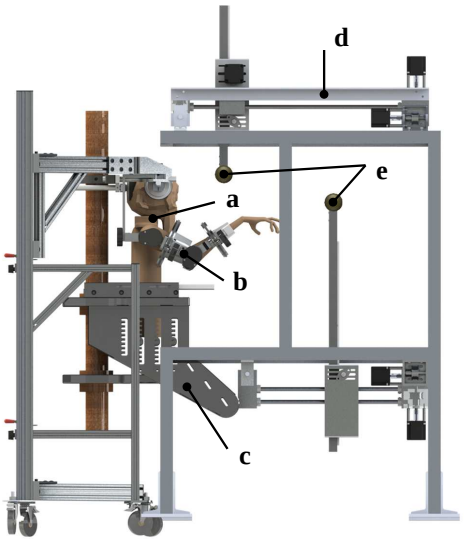

FIGURE 4: DESIGNED 3D BMI TASK FOR A MACAQUE SUBJECT. (a. macaque, b. exoskeleton, c. primate chair, d. 3D presentation system, e. targets)

TABLE 1: KEY UPPER-LIMB DIMENSIONS COMPARING BMI MACAQUES[1] VS. HUMANS

	Length (cm)		Circumference (cm)	
Subjects	Upper arm	Forearm[a]	Upper arm	Forearm
Macaque G	14.5	15.2	23.2	16.2
Macaque J	13.7	16.2	24.5	18.0
Macaque W	14.2	16.3	23.5	17.1
Human	37.4[b]	48.8[b]	31.8[c]	24.2[c]

[a] from elbow to hand.
[b] average of male and female data from [18].
[c] data from [19].

ponents of the exoskeleton should be kept sufficiently compact, and some complex designs good for adult humans may not be applicable to macaques with relatively smaller body dimensions.

Joint ROM and Workspace Since the macaque joint ROMs are not available in existing literatures, human physiological and ADL ROMs are referenced (in the third and the fourth column of Table 2, averaged from [10, 14, 20]), which are sufficient to cover the workspace (in front of the coronal plane of macaque body) of macaques in the proposed BMI tasks. Additionally, it is assumed that the elevation/depression and protraction/retraction of the macaque shoulder are negligible during BMI task motions.

[1]Three adult male rhesus macaques (Macaca mulatta) were used in this study. All procedures were conducted in compliance with the National Institute of Health Guide for Care and Use of Laboratory Animals and were approved by the University of California, Berkeley Institutional Animal Care and Use Committee.

TABLE 2: HUMAN ROM AND THE DESIGNED MECHANICAL LIMITS.

Joint	Motion	Phy. ROM	ADL ROM	Mech. Limit
1	azi. add./abd.	–	170°	191.0°
2	shld. add./abd.	182°	145°	276.6°
3	shld. flx./ext.	249°	110°	196.2°
4	shld. int./ext.	187°	150°	160.0°
5	elbw. int./ext	142°	140°	96.8°
6	pron./supi.	190°	135°	160.0°

Mechanical Design

Shoulder Joint DOF Assignment Kinematically redundant mechanisms enjoy flexibility in positioning and tracking due to their possession of more DOFs than required. Accordingly, a 6-DOF upper limb exoskeleton design is proposed in Fig. 5. 4 DOFs are assigned to the shoulder complex by integrating the azimuthal rotation joint from convention (b) (Fig. 2) to the whole triad model in convention (a). With an extra DOF at the shoulder joint, better mechanism manipulating ability can be achieved. The elbow joint and the radioulnar joint are each modeled by one single DOF.

Prosthetic Joint Design Exoskeletons are supposed to be wearable, and thus the prosthetic joints of an upper limb exoskeleton can be classified into two types: one with rotation axis being perpendicular to the arm segments (Joint 1, 2, 3, and 5, Fig. 6a), and the other one with rotation axis being along the longitude of the arm segments (Joint 4 and 6, Fig. 6b). Two cuffs 3D-printed following macaque arm morphology with elastic braces are used to attach the exoskeleton to the macaque arm, and an opening is left for each cuff for easy attachment as well as avoiding collision between the exoskeleton and macaque body. A curved guide rail, a sliding roller with bearing groups, and a timing belt with pulley are mounted on the cuff to transmit the upper/lower arm's rotation movement to the sensors.

Designed Joint ROM Compared with human ADL ROM, most designed mechanical joint limits (listed in the last

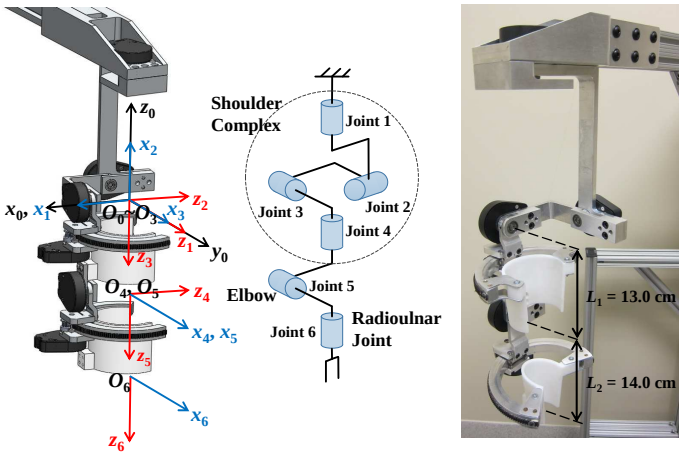

FIGURE 5: LEFT: CAD model with coordinate frames in exoskeleton home posture. MIDDLE: Simplified joint model. RIGHT: Physical hardware design implementation.

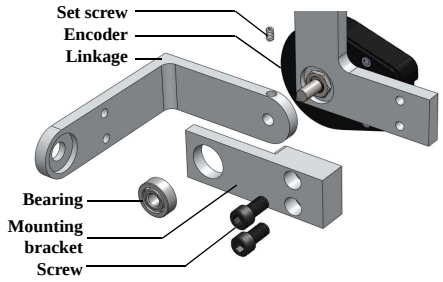

(a) JOINT TYPE I

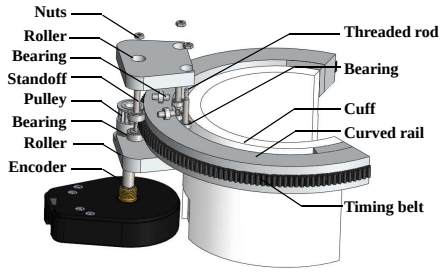

(b) JOINT TYPE II

FIGURE 6: CAD DESIGN OF TWO TYPES OF JOINTS.

column of Table 2) meet the design requirements. In the designed reach and press task with button-controlled LEDs being the targets, since the BMI task workspace is prescribed as always in front of macaque's coronal plane and does not involve elbow flexion of over 90°, the designed ROMs of each joint satisfy the specified requirements. Additionally, two sets of linkages with different lengths will be used for different sized subjects on the current stage, and a linkage length adjustment feature will be

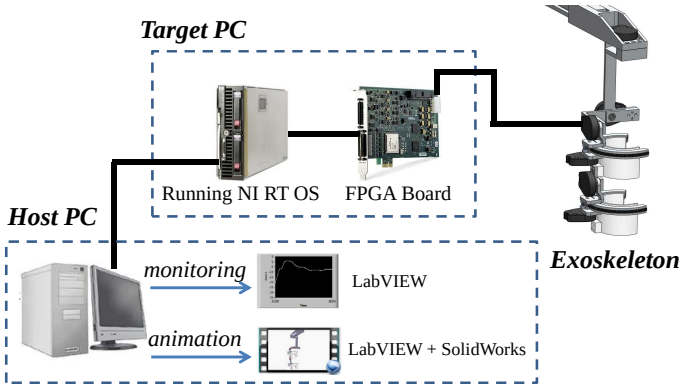

FIGURE 7: STRUCTURE OF THE REAL-TIME DATA ACQUISITION OF THE EXOSKELETON SYSTEM.

TABLE 3: DH PARAMETERS OF THE PROPOSED UPPER LIMB EXOSKELETON.

Joint	θ	d	a	α
1	θ_1	0	0	$-90°$
2	$\theta_2 - 90°$	0	0	$90°$
3	$\theta_3 + 90°$	0	0	$-90°$
4	θ_4	L_1	0	$90°$
5	θ_5	0	0	$-90°$
6	θ_6	L_2	0	$0°$

added to the next generation of an actuated exoskeleton design.

Real-Time Data Acquisition Setup

For real-time data acquisition, a target PC consisting of an NI FPGA board running real-time and FPGA modules is used for collecting data from the encoders, and a host PC acts as a terminal for monitoring/analyzing the data acquisition process, as shown in Fig. 7.

KINEMATIC MODELING AND ANALYSIS

System Kinematic Model

Denavit-Hartenberg (DH) parameters can fully define the kinematic model of a mechanism. Let $\boldsymbol{\theta} \in \mathbb{R}^6$ be the joint variable (joint rotation position). Then DH parameters of the proposed 6-DOF exoskeleton model are as shown in Table 3 following the frame definition in Fig. 5, where L_1 and L_2 are the distance from the shoulder center to the elbow, and the distance from the elbow to the end point, respectively. The posture at $\boldsymbol{\theta} = \mathbf{0}$ is defined as the *home posture* of the exoskeleton.

Singularity and Manipulability of Shoulder Joint

Singularity The Jacobian matrix loses rank at singularities. For the ball-and-socket shoulder joint model with fixed upper arm length, the end point moves on a spherical surface. Thus the orientation Jacobian $\boldsymbol{J}_o(\boldsymbol{\theta})$ that maps the angular velocities of the first four joints to the elbow's task space angular velocities is derived as

$$\boldsymbol{J}_o(\boldsymbol{\theta}) = \begin{bmatrix} 0 & -s_1 & c_1 s_2 & -c_1 c_2 s_3 - s_1 c_3 \\ 0 & c_1 & s_1 s_2 & -s_1 c_2 s_3 + c_1 c_3 \\ 1 & 0 & c_2 & s_2 s_3 \end{bmatrix} \tag{1}$$

where $s_i = \sin(\theta_i)$, and $c_i = \cos(\theta_i)$. $\boldsymbol{J}_o(\boldsymbol{\theta})$ becomes rank-deficient at $(\theta_2, \theta_3) = (-\pi, 0)$, the only singularity in the workspace of the proposed shoulder model. However, the same posture of this singular point can be realized by other joint space configurations due to the redundant DOF, therefore providing the ability of singularity avoidance.

Manipulability To quantitatively evaluate the mechanism's manipulation ability, the measure of *manipulability* [21] can be defined as

$$w(\boldsymbol{\theta}) = \sqrt{\det(\boldsymbol{J}(\boldsymbol{\theta})\boldsymbol{J}^{\top}(\boldsymbol{\theta}))}. \tag{2}$$

The manipulability provides a measure of the dexterity of the exoskeleton given a joint space configuration. Since the mapping from the joint space to the task space may not be unique, in particular, for redundant mechanisms, the manipulability of a particular task space point may not be unique. Thus we introduce the terminology *manipulability distribution* here to define the range of values for manipulability. The performance of the exoskeleton on the horizontal plane (i.e., the $x_0O_0y_0$ plane defined in Fig. 5) is important considering the designed BMI tasks previously discussed. Fig. 8 shows the manipulability distribution on the horizontal plane of our proposed shoulder complex model, as well as an illustration of the manipulability study with the elbow position as the investigated end point. This redundant realization makes it possible to obtain the maximal manipulability value ($\max_{\theta_2,\theta_3}\{\text{Eq. (2)}\} = \sqrt{2}$) in all directions on the horizontal plane, and each posture possesses different levels of manipulabilities. Thus it is possible to avoid its singularity by appropriately planning its joint space trajectories. Further kinematic analysis of the feasibility for this shoulder model to avoid singularity and joint limits can be found in our previous work [22], and gradient projection method can be one solution to realize kinematic control and singularity avoidance for an actuated redundant robot manipulator [23].

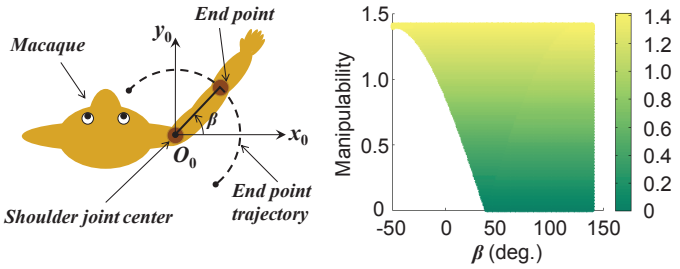

FIGURE 8: LEFT: Macaque plotted with its shoulder joint center fixed and elbow as the end point. RIGHT: Manipulability distribution of the proposed shoulder joint model on the horizontal plane; manipulability takes any value in the colored region and the white region represents no value.

SYSTEM KINEMATIC CALIBRATION

Considering the relatively low accuracy of most state-of-the-art neural decoders [24], the positioning accuracy requirement (within 10 mm) of the palm center in the BMI study is considerably lower than general industrial robots. Here we choose US Digital S6 incremental optical encoder with 2500 counts per round for each joint, and encoder indices are utilized for indicating the reference positions.

For the current setup, position measurement error comes from two major sources – unknown encoder value offsets at exoskeleton home posture and kinematic model uncertainties. Kinematic calibration needs to be conducted to reduce the position measurement error. An external optical tracking system is an ideal candidate for providing 3D position information as the reference true value. By comparing the position data in the tracking system frame and the exoskeleton frame, the unknown variable values can be identified using an optimization-based approach. Note, this is an offline process, which only needs to be conducted once before the exoskeleton is put into use.

Calibration Setup

Our optical tracking setup is the *PhaseSpace IMPULSE X2 Motion Capture System* consisting of 10 cameras with sampling rate of 480 Hz. This system can track its active LED markers and has sub-millimeter accuracy [25]. To acquire the position information of the exoskeleton, one marker was rigidly attached to the end point of the last link (Fig. 9). We moved the end point along some arbitrary trajectory in the task space during which all six joints were involved as much as possible. The position of the marker was recorded by the motion capture system, and the joint space motion by each encoder. The sampling rate of the encoder reading is 1 kHz, and the two data acquisition systems were synchronized via Network Time Protocol (NTP).

Calibration Algorithm

Calibration algorithm for the j-th sampling step is shown in Fig. 10 (variables in red are to be identified). Define $\Delta\boldsymbol{\theta}^0 \in \mathbb{R}^6$ as the vector of all six encoder offsets at exoskeleton's home posture. Together with encoder readings $\boldsymbol{\theta}^{R,j}$, the joint space variable $\boldsymbol{\theta}^j$ can be expressed as

$$\boldsymbol{\theta}^j = \Delta\boldsymbol{\theta}^0 + \boldsymbol{\theta}^{R,j} \tag{3}$$

Introduce $\Delta\boldsymbol{p}^M \in \mathbb{R}^3$ as the marker's coordinates deviation from its nominal and actual value in the O_6-$x_6y_6z_6$ frame (following the definition in Fig. 5). Then we can obtain the marker position in the exoskeleton's frame $\boldsymbol{p}^j_{\text{exo}}$ via coordinate transformation matrix $\boldsymbol{T}^0_6(\Delta\boldsymbol{\zeta}, \boldsymbol{\theta}^j)$ by forward kinematics, where $\Delta\boldsymbol{\zeta} := [\Delta d_2, \Delta d_3, \Delta d_5, \Delta a_3, \Delta a_5]^\top \in \mathbb{R}^5$ represents the vector of the concerned deviations of the exoskeleton nominal DH parameters from their actual values. Besides, as shown in Fig. 9, the relative posture between the camera frame and the exoskeleton frame is not exactly known, and thus two additional variables $\boldsymbol{d} \in \mathbb{R}^3$ and $\boldsymbol{\varphi} \in \mathbb{R}^3$ are needed to represent the relative translations and rotations (Euler angles) between the two frames, respectively. The marker's coordinates in the camera frame $\boldsymbol{p}^j_{\text{cam}}(\Delta\boldsymbol{\theta}^0, \Delta\boldsymbol{\zeta}, \Delta\boldsymbol{p}^M, \boldsymbol{d}, \boldsymbol{\varphi})$ can be then obtained through the frame transformation matrix $\boldsymbol{A}^{\text{cam}}_{\text{exo}}(\boldsymbol{d}, \boldsymbol{\varphi})$ with knowledge of the encoder information. On the other hand, the marker's coordinates in the camera frame $(\boldsymbol{p}^j_{\text{cam}})^*$ can be directly acquired by the cameras, which serve as the reference in this calibration process. Thus the position error is

$$e^j = ||(\boldsymbol{p}^j_{\text{cam}})^* - \boldsymbol{p}^j_{\text{cam}}(\Delta\boldsymbol{\theta}^0, \Delta\boldsymbol{\zeta}, \Delta\boldsymbol{p}^M, \boldsymbol{d}, \boldsymbol{\varphi})||_2 \tag{4}$$

Select N calibration points along the trajectory, and define $\boldsymbol{x} := [(\Delta\boldsymbol{\theta}^0)^\top, (\Delta\boldsymbol{\zeta})^\top, (\Delta\boldsymbol{p}^M)^\top, \boldsymbol{d}^\top, \boldsymbol{\varphi}^\top]^\top$ as the parameter vector to be identified. Then the calibration algorithm can be cast as the following optimization problem

$$\begin{aligned} \min_{\boldsymbol{x}} \quad & \textstyle\sum_{j=1}^{N} ||(\boldsymbol{p}^j_{\text{cam}})^* - \boldsymbol{p}^j_{\text{cam}}(\boldsymbol{x})||_2^2 \\ \text{s.t. } & x_i^L \le x_i \le x_i^U, \quad i = 1, 2, \ldots, 20. \end{aligned} \tag{5}$$

where x_i^L is the lower bound of the corresponding element, and x_i^U the upper bound. This is a typical nonlinear least squares problem, and can be solved using the `lsqnonlin` command in the MATLAB Optimization Toolbox [26].

Experiment Results and Analysis

Parameter Identification 400 data points are downsampled in one experiment session for parameter training. Figure 11 shows the comparison between data fitting results before and after calibration with the blue lines representing the position errors. The identification results and initial guesses (nominal mechanical design values) are listed in Table 4. The calibrated root-mean-square (RMS) position error of this training dataset is 1.05 mm, with mean of 0.95 mm and standard deviation of 0.44 mm.

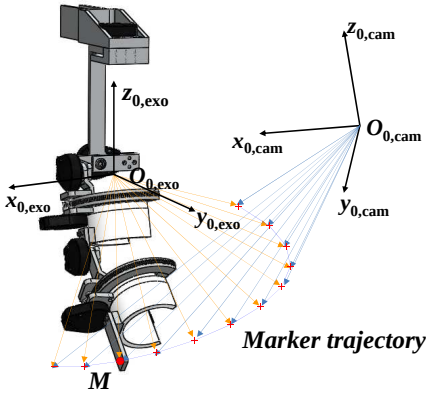

FIGURE 9: ILLUSTRATION OF SYNCHRONIZED DATA ACQUISITION OF THE EXOSKELETON SYSTEM AND THE MOTION CAPTURE SYSTEM.

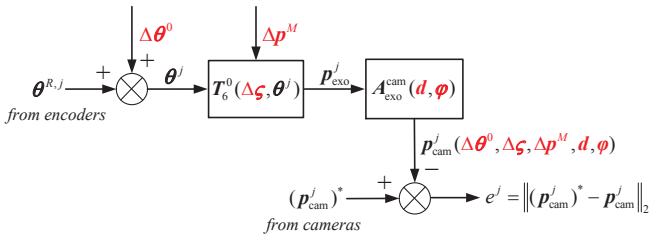

FIGURE 10: BLOCK DIAGRAM OF THE PROPOSED CALIBRATION ALGORITHM.

Cross-Validation To evaluate the identification results obtained from one certain dataset, cross-validations are conducted using six datasets of 300 data points downsampled from other experiment sessions. Position errors of the cross-validation and the training datasets are given in Fig. 12. We can notice that the position errors of the cross-validation datasets are approximately of the same level as the training dataset, which indicates that the calibration results in Table 4 are fairly satisfactory considering the position accuracy requirement of the BMI tasks.

CONCLUSIONS AND FUTURE WORK

A 6-DOF passive macaque upper limb exoskeleton was proposed and fabricated for a BMI study. 4 DOFs were assigned at the shoulder joint to achieve redundancy for kinematic sin-

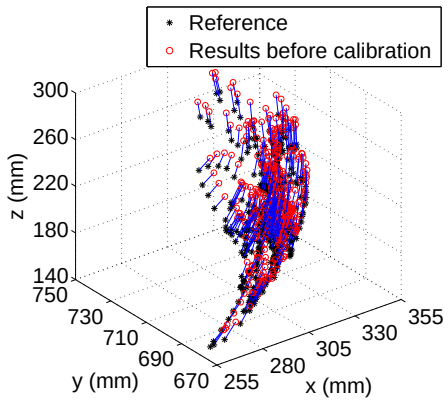

(a) BEFORE CALIBRATION

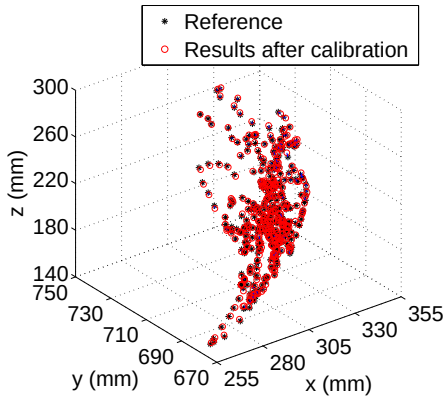

(b) AFTER CALIBRATION

FIGURE 11: SAMPLED MARKER POSITIONS IN THE CAMERA FRAME FOR REFERENCE DATA AND GENERATED DATA BEFORE/AFTER CALIBRATION.

gularity avoidance. A kinematic model of the proposed design was established, and manipulability analysis demonstrated the model's ability to avoid singularity for the shoulder complex model. Real-time data acquisition of the exoskeleton system was set up, and approximately 2 mm end point sensing position accuracy was achieved by kinematic calibration. For immediate future work, kinematic motion data acquisition will be conducted with a pilot macaque to test the performance of the proposed exoskeleton in terms of DOF assignment, which in turn will provide guidance for future joint axis alignment study. Additionally, an actuated version of a cable-driven macaque upper limb exoskeleton with back-drivable and force-reflecting joints is currently in progress.

TABLE 4: EXPERIMENTAL RESULTS OF THE PROPOSED IDENTIFICATION APPROACH.

para.	guess	result	para.	guess	result
$\Delta\theta_1^0$ (deg.)	30.7	31.85	Δa_5 (mm)	0	0.03
$\Delta\theta_2^0$ (deg.)	−16.3	−17.60	Δp_x^M (mm)	0	−0.10
$\Delta\theta_3^0$ (deg.)	−15.2	−13.45	Δp_y^M (mm)	0	−0.16
$\Delta\theta_4^0$ (deg.)	−17.1	−17.19	Δp_z^M (mm)	0	−8.46
$\Delta\theta_5^0$ (deg.)	−25.5	−22.11	d_x (mm)	203.2	203.29
$\Delta\theta_6^0$ (deg.)	−2.3	−2.39	d_y (mm)	852.1	849.31
Δd_2 (mm)	0	−1.79	d_z (mm)	216.8	224.30
Δd_3 (mm)	0	−0.48	φ_x (deg.)	−90.0	−89.01
Δd_5 (mm)	0	2.80	φ_y (deg.)	0	−0.10
Δa_3 (mm)	0	−4.01	φ_z (deg.)	−135.0	−135.52

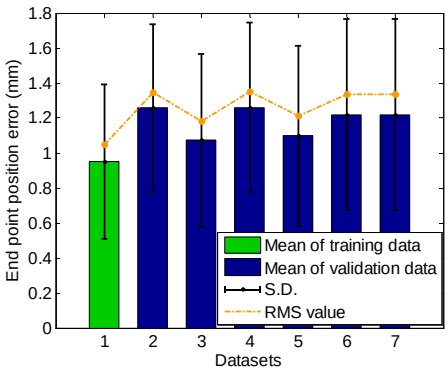

FIGURE 12: POSITION ERRORS OF BOTH TRAINING AND CROSS-VALIDATION DATASETS.

ACKNOWLEDGMENT

We would like to thank Dr. Joonbum Bae for his early effort on this project. We also want to thank Dr. Simon Overduin and Suraj Gowda for their discussions on this work from the BMI study aspect, Dr. Gregorij Kurillo and Robert Matthew for their help in system calibration, and Dennis Lee and Mick Franssen for their assistance in the hardware fabrication.

REFERENCES

[1] Velliste, M., Perel, S., Spalding, M. C., Whitford, A. S., and Schwartz, A. B., 2008. "Cortical control of a prosthetic arm for self-feeding". *Nature*, ***453***, pp. 1098–1101.

[2] Hochberg, L. R., Bacher, D., Jarosiewicz, B., Masse, N. Y.,

Simeral, J. D., Vogel, J., Haddadin, S., Liu, J., Cash, S. S., van der Smagt, P., and Donoghue, J. P., 2012. "Reach and grasp by people with tetraplegia using a neurally controlled robotic arm". *Nature,* ***485***, pp. 372–375.

[3] Nef, T., and Riener, R., 2008. "Shoulder Actuation Mechanisms for Arm Rehabilitation Exoskeletons". In Proc. IEEE/RAS-EMBS Int. Conf. on Biomed. Robot. Biomechatronics (BioRob), pp. 862–868.

[4] Tonet, O., Marinelli, M., Citi, L., Rossini, P. M., Rossini, L., Megali, G., and Dario, P., 2008. "Defining brain-machine interface applications by matching interface performance with device requirements". *J. Neurosci. Methods,* ***167***(1), pp. 91–104.

[5] Millan, J. R., and Carmena, J. M., 2010. "Invasive or non-invasive: Understanding brain-machine interface technology". *IEEE Eng. Med. Biol. Mag.,* ***29***(1), pp. 16–22.

[6] Scott, S. H., 1999. "Apparatus for measuring and perturbing shoulder and elbow joint positions and torques during reaching". *J. Neurosci. Methods,* ***89***(2), pp. 119–127.

[7] Gopura, R. A. R. C., and Kiguchi, K., 2009. "Mechanical designs of active upper-limb exoskeleton robots: State-of-the-art and design difficulties". In Proc. IEEE Int. Conf. on Rehabil. Robot. (ICORR), pp. 178–187.

[8] Wu, G., van der Helm, F. C. T., Veeger, H. E. J., Makhsous, M., van Roy, P., Anglin, C., Nagels, J., Karduna, A. R., McQuade, K., Wang, X., Werner, F. W., and Buchholz, B., 2005. "ISB recommendation on definitions of joint coordinate systems of various joints for the reporting of human joint motion - Part II: shoulder, elbow, wrist and hand". *J. Biomechanics,* ***38***, pp. 981–992.

[9] Ball, S., Brown, I., and Scott, S., 2007. "MEDARM: a rehabilitation robot with 5DOF at the shoulder complex". In Proc. IEEE/ASME Int. Conf. Adv. Intell. Mech. (AIM), pp. 1–6.

[10] Ergin, M. A., and Patoglu, V., 2012. "ASSISTON-SE: A self-aligning shoulder-elbow exoskeleton". In Proc. IEEE Int. Conf. Robotics Autom. (ICRA), pp. 2479–2485.

[11] Medical Multimedia Group, 2008. Image used courtesy of Medical Multimedia Group, LLC. URL `http://www.eorthopod.com`.

[12] Romilly, D. P., Anglin, C., Gosine, R. G., Hershler, C., and Raschke, S. U., 1994. "A Functional Task Analysis and Motion Simulation for the Development of a Powered Upper-Limb Orthosis". *IEEE Trans. Rehabil. Eng.,* ***2***(3), pp. 119–129.

[13] Cheng, E. J., and Scott, S. H., 2000. "Morphometry of Macaca mulatta forelimb. I. Shoulder and elbow muscles and segment inertial parameters". *J. of Morphology,* ***245***(3), pp. 206–224.

[14] Perry, J., Rosen, J., and Burns, S., 2007. "Upper-Limb Powered Exoskeleton Design". *IEEE/ASME Trans. Mechatronics,* ***12***(4), Aug., pp. 408–417.

[15] Letier, P., Avraam, M., Veillerette, S., Horodinca, M., Bartolomei, M. D., Schiele, A., and Preumont, A., 2008. "SAM: A 7-DOF portable arm exoskeleton with local joint control". In Proc. IEEE/RSJ Int. Conf. Intell. Robots Syst. (IROS).

[16] Christel, M. I., and Billard, A., 2002. "Comparison between macaques' and humans' kinematics of prehension: the role of morphological differences and control mechanisms". *Behavioural Brain Research,* ***131***(1-2), pp. 169–184.

[17] Yang, J., Abdel-Malek, K., and Nebel, K., 2005. "Reach Envelope of a 9-Degree-of-Freedom Model of the Upper Extremity". *Int. J. Robot. Autom. (IJRA),* ***20***(4), pp. 240–259.

[18] Huston, R., 2009. *Principles of Biomechanics.* Taylor & Francis CRC Press.

[19] Schell, K., Bradley, E., Bucher, L., Seckel, M., Lyons, D., Wakai, S., Bartell, D., Carson, E., Chichester, M., Foraker, T., and Simpson, K., 2006. "Clinical Comparison of Automatic, Noninvasive Measurements of Blood Pressure in the Forearm and Upper Arm". *Am. J. Crit. Care,* ***15***(2), pp. 196–205.

[20] Cott, H. P. V., and Kinkade, R. G., 1972. *Human Engineering Guide to Equipment Design*, revised ed. McGraw-Hill, Washington D. C., U.S.A.

[21] Yoshikawa, T., 1985. "Manipulability of Robotic Mechanisms". *Int. J. Robotics Research (IJRR),* ***4***(2), pp. 3–9.

[22] Lu, J., Chen, W., and Tomizuka, M., 2013. "Kinematic Design and Analysis of a 6-DOF Upper Limb Exoskeleton Model for a Brain-Machine Interface Study". In Proc. 6th IFAC Symp. on Mechatronic Syst., pp. 293–300.

[23] Siciliano, B., 1990. "Kinematic control of redundant robot manipulators: A tutorial". *J. Intell. Robot. Syst.,* ***3***, pp. 201–212.

[24] Shanechi, M. M., Williams, Z. M., Wornell, G. W., Hu, R. C., Powers, M., and Brown, E. N., 2013. "A Real-Time Brain-Machine Interface Combining Motor Target and Trajectory Intent Using an Optimal Feedback Control Design". *PLoS ONE,* ***8***(4), 04, p. e59049.

[25] PhaseSpace Inc., 2012. The IMPULSE X2 Motion Capture System Catalog. URL `http://www.phasespace.com`.

[26] MathWorks, 2012. Optimization Toolbox. URL `http://www.mathworks.com`.